J. Biochem. 2011;149(6):673–684 doi:10.1093/jb/mvr015

JB THE JOURNAL OF BIOCHEMISTRY

Homology modelling and site-directed mutagenesis studies of the epoxide hydrolase from *Phanerochaete chrysosporium*

Received January 19, 2011; accepted January 26, 2011; published online February 3, 2011

Lin-Feng Zhang, Jin-Ming Wu and Hong Feng*

Key Laboratory of Bio-resources and Eco-environment of Ministry of Education, Sichuan Key Laboratory of Molecular Biology and Biotechnology, College of Life Sciences, Sichuan University, Chengdu, Sichuan, P. R. China, 610064

*Hong Feng, Key Laboratory of Bio-resources and Eco-environment of Ministry of Education, Sichuan Key Laboratory of Molecular Biology and Biotechnology, College of Life Sciences, Sichuan University, Chengdu, Sichuan, P. R. China, 610064. Tel: 86-28-85412738, Fax: 86-28-85412738, email: hfeng@scu.edu.cn

Three-dimensional structural model of epoxide hydrolase (PchEHA) from *Phanerochaete chrysosporium* was constructed based on X-ray structure of *Agrobacterium radiobacter* AD1 sEH using SWISS-MODEL server. Conserved residues constituting the active site cavity were identified, of which the functional roles of 14 residues were determined by site-directed mutagenesis. In catalytic triad, Asp105 and His308 play a leading role in alkylation and hydrolysis steps, respectively. Distance between Asp105 and epoxide ring of substrate may determine the regiospecificity in the substrate docking model. Asp277 located at the entrance of substrate tunnel is concerned with catalysis but not essential. D307E had the highest activity and lower enantioselectivity among 14 mutants, suggesting Asp307 may be involved in choice of substrate configuration. Y159F and Y241F almost exhibited no activity, indicating that they are essential to bind substrate and facilitate opening of epoxide ring. Besides, His35–Gly36–Asn37–Pro38, Trp106 and Trp309 surrounding Asp105, may coordinate the integration of active site cavity and influence substrate binding. Especially, W106I reversed the enantioselectivity, perhaps due to more deteriorative impact on the preferred (*R*)-styrene oxide. Gly65 and Gly67 occurring at β-turns and Gly36 are vital in holding protein conformation. Conclusively, single conserved residue around the active sites has an important impact on catalytic properties.

Keywords: docking/epoxide hydrolase/homology modelling/*Phanerochaete chrysosporium*/site-directed mutagenesis.

Abbreviations: EHs, epoxide hydrolases; mEH, microsomal epoxide hydrolase; PchEHA, epoxide hydrolase from *Phanerochaete chrysosporium*; sEH, soluble epoxide hydrolase; wt, wild-type.

Epoxide hydrolases (EHs, EC3.3.2.3) are ubiquitous enzymes that convert epoxides to their corresponding vicinal diols by addition of a water molecule. They have been gained considerable attention in recent years due to their roles in the detoxification, catabolism and regulation of signalling molecules (*1–3*). Moreover, the observed intrinsic enantioselectivity of some EHs makes them useful in the preparation of enantiopure pharmaceuticals and other fine chemicals (*4*).

To facilitate large-scale industrial application, studies have been focused on the cloning, expression, purification, characterization, catalytic mechanism, modification of activity and enantioselectivity, resolution of structure and homology modelling of various EHs (*5–14*). Knowledge of more than 100 EHs sequences suggests that most EHs belong to the α/β-fold hydrolase family (*15*, *16*). The structure has been experimentally determined for several EHs from *Agrobacterium radiobacter* AD1, *Aspergillus niger*, *Mycobacterium tuberculosis*, *Solanum tuberosum*, *Mus musculus* and *Homo sapiens* (*7*, *11*, *12*, *17–19*). These enzymes share a common framework: a core domain composed of the central β-sheets surrounded by α-helices and a variable cap domain positioned on the top (*15*). On the whole, the structural difference is the length of two loops: the NC-loop connecting the core and the cap domain and the cap-loop that is inserted into the cap domain (*16*). EHs use a catalytic mechanism that involves an Asp–His–Asp/Glu (nucleophile–histidine–acid) catalytic triad located between the core and the cap domain (*1–3*, *15*, *20*). The catalytic process can be divided into two steps: alkylation and hydrolysis. First, the nucleophile opens the epoxide ring by nucleophilic attack and a covalently bound ester intermediate is formed rapidly. Second, the histidine–acid pair activates a water molecule that hydrolyses the alkyl–enzyme intermediate and then releases the product. The catalytic process is assisted with two tyrosine residues serving as proton donors and the oxyanion hole stabilizing the negative charge on the carbonyl oxygen of the nucleophilic aspartate (*3*, *20*). Although the common mechanism is known, many fine details, such as the molecular basis of substrate selectivity, remain to be understood. A few methods, including 'rational designed' site-directed mutagenesis, saturation mutagenesis, error-prone polymerase chain reaction (PCR) and DNA shuffling, have been applied to enhance the activity and enantioselectivity of EHs (*9*, *21–27*). Through high-throughput screening, many functional

improved EH mutants have been obtained, which shows a good prospect for EHs in biotechnological application.

The epoxide hydrolase (PchEHA) from white-rot basidiomycetes *Phanerochaete chrysosporium*, belonging to soluble EHs, can catalyse the hydrolysis of several epoxides to their corresponding diols and has been shown good potentials in resolution of racemic epoxides (*28*). In the context of our previous work regarding PchEHA, we report in this article its homology modelling, substrate docking, active site cavity and the conserved residues relating to the enzymatic function via site-directed mutagenesis. These findings could be the basis for further studies and synthetic applications.

Materials and Methods

Materials

All chemicals were reagent grade commercial products and used without further purification. Epoxides were purchased from Kely Bio-Pharmaceutical Co. (Shanghai, China), except for racemic and (*S*)-styrene oxide (SO) from Sigma-Aldrich Co. (USA). *Pfu* DNA polymerase was purchased from Tiangen Biotech Co. (Beijing, China). *Dpn* I was from Fermentas (Canada). The HisTrap FF Crude 1 ml column was from GE Healthcare (St Louis, USA). *Escherichia coli* strain JM109 served as the host for cloning. *Escherichia coli* BL21 (DE3) (Novagen, Gibbstown, USA) was used for gene expression.

Homology modelling of PchEHA and substrate docking

The conserved features of PchEHA were compared with other soluble EHs by multiple sequence alignment using Clustalx1.83 program. The 3D coordinates of PchEHA was generated with SWISS-MODEL Server using the X-ray crystallographic structure of *A. radiobacter* AD1 sEH (PDB code: 1ehyA) as the template and visualized with Swiss-PdbViewer 3.7 (*29–31*). Based on the structural model, mutants of PchEHA were constructed and analysed by Swiss-PdbViewer 3.7.

Substrate docking was performanced based on the homology model using iGEMDOCK v2.1 (*32*, *33*). The (*R*)- and (*S*)-SO were docked into the active cavity of PchEHA model.

Site-directed mutagenesis

The site-directed mutagenesis was carried out following the QuikChange protocol with the specific primers (See Supplementary Data, Table S1). The expression plasmid pE28EHA [pET-28a (+) hosting the gene encoding PchEHA] (*28*) was used as the template for construction of the mutation genes. The mutagenesis PCR was performed with *Pfu* DNA polymerase using a program of 1 min at 95°C followed by 30 cycles of 95°C for 40 s, 68°C for 8 min and a final extension at 68°C for 10 min. The restriction enzyme *Dpn* I was directly added to the PCR reaction tube to degrade the methylated template for 1 h at 37°C. The PCR products were purified and transformed into *E. coli* JM109 and cultivated on the LB (Luria–Bertani) agar plate containing 50 μg/ml kanamycin. The constructs were confirmed by DNA sequencing using the T7 forward and reverse primer. And the verified plasmid was transformed into *E. coli* BL21 (DE3) for over-expression.

Protein expression and purification

The recombinant *E. coli* clone hosting each desired mutation gene was cultivated at 37°C and 200 rpm orbital shaking in 1 l of LB broth containing 50 μg/ml kanamycin. After the cells reached an OD_{600} of 0.4–0.6, protein over-expression was induced fully with 0.5 mM isopropyl-β-D-thiogalactoside (IPTG) and the culture was continuously incubated at 18°C for additional 16 h. The cells were harvested by centrifugation at 2,000*g* for 10 min at 4°C. Cell pellet was resuspended in 40 ml disruption buffer [20 mM K_2HPO_4/KH_2PO_4, pH 8.0, 250 mM NaCl, 0.5 mM phenylmethylsulphonyl fluoride (PMSF) and 10% glycerol] and sonicated using an ultrasonic homogerizer sonicator (Cole-Parmer, Vernon Hills, USA) on ice bath. The lysate was clarified at 3,300*g* for 10 min at 4°C to remove the cell debris. The supernatant was applied to immobilized metal ion affinity chromatography using ÄKTA Prime System (Amersham, San Francisco, USA) as described previously (*28*). The fusion protein that specifically bound to the HisTrap FF Crude 1 ml column was eluted with 0–500 mM imidazole. The fractions corresponding to the absorption peak at 280 nm were pooled and dialysed against 100 volumes of dialysis buffer [10 mM K_2HPO_4/KH_2PO_4, pH 8.0, 0.5 mM DTT and 0.1 mM ethylenediaminetetracetic acid (EDTA)] at 4°C overnight. Afterward, the samples were lyophilized and stored at 4°C. Before activity assay, the powder of purified enzymes were dissolved in the 0.1 M K_2HPO_4/KH_2PO_4 buffer (pH 8.0) and kept at 4°C for short time. Protein purity was monitored by SDS–PAGE (12.5%) and the concentration was quantified using AlphaImager software (Alpha Innotech Corporation, San Leandro, USA) with 0.1% bovine serum albumin (BSA) as a standard.

Activity assays

When (*R*)- and (*S*)-glycidyl tosylate (GT) were used as the substrates, the epoxide- hydrolase activity assays were based on a chromogenic reaction of epoxide with 4-nitrobenzylpyridine (*34*, *35*). This reaction produces a blue colour, the intensity of which is proportional to the amount of epoxide. Each of purified PchEHA wild-type (wt) and mutant enzymes (20 μg) were brought into contact with 12 mM GT in 50 μl of 0.1 M phosphate buffer (pH 8.0) at 37°C for 1 h. Then, 50 μl of reagent A [50 mM 4-nitrobenzylpyridine in 80% ethylene glycol and 20% acetone (v/v)] was added. The reaction mixture was heated at 80°C for 10 min. After cooling to the room temperature, 40 μl of the mixture was diluted into 560 μl of 0.1 M phosphate buffer (pH 8.0). Before measuring the OD value at 565 nm with spectrophotometer UV-2450 (Shimadzu, Tokyo, Japan), 200 μl of reagent B [50% triethylamine and 50% acetone (v/v)] was added.

In addition, the hydrolytic activity towards racemic, (*R*)- and (*S*)-SO was determined by another spectrophotometric method (*36*). It was based on the chemical oxidation of diol with sodium metaperiodate ($NaIO_4$), the resulting product of benzaldehyde had a strong UV absorbency at 290 nm ($\varepsilon = 1356/M/cm$). The purified enzymes (15 μg per assay) were mixed with 32 mM SO in 50 μl of 10 mM phosphate buffer (pH 8.0) containing 4% dimethyl sulphoxide (DMSO) at 37°C. After 30 min, the hydrolytic reaction was immediately stopped by heated at 90°C for 5 min. Finally, 742 μl of 10 mM phosphate buffer (pH 8.0) and 8 μl of 200 mM $NaIO_4$ were added. The benzaldehyde was quantified at 290 nm.

The enzymatic activities were calculated according to the standard curve made in the same procedure as above with each substrate in a range of various concentrations. All the activity assays were carried out at least ×3 three times.

Determination of kinetic properties

For the purified wt and mutants of H35P, N37W, W106I, D277E, D307G, W309A, the steady-state kinetic parameters for racemic, (*R*)- and (*S*)-SO were determined spectrophotometrically by the end-point measurements of benzaldehyde as described above (*36*). The initial velocity was measured at substrate concentration ranging from 10 mM to 80 mM with 20 μg of the purified enzyme. The data were used to calculate K_m and V_{max} values by non-linear regression analysis. The catalytic constant k_{cat} was deduced using a molecular mass of 41 kDa. All parameters were calculated using the mean values from three independent experiments. The *E*-value, corresponding to the enantioselectivity of the enzyme, was derived from the ratio of k_{cat}/K_m of the separate enantiomers (*37*).

For the other mutants that showed lower activities, the hydrolytic course of SO was performed on the spectrometer by online monitoring of the formation of benzaldehyde at 290 nm (*34*). In a 100 μl cell, 86 μl of 10 mM phosphate buffer (pH 8.0), 2 μl of SO solution (100 mM in DMSO) and 2 μl of 100 mM $NaIO_4$ solution were mixed. The mixture was equilibrated at 37°C for 3 min, 10 μl of enzyme (5 μg/μl) was then added to initiate the enzymatic hydrolysis. The reactive course of 15 min was recorded. The *E*-value was roughly estimated by the ratio of two initial velocities of the hydrolytic course of the separate enantiomers (*38*). All the assays were done in duplicate or triplicate.

Results

Homology modelling and substrate docking

For getting more insights into the catalytic mechanism and the enantioselectivity of the PchEHA from *P. chrysosporium*, homology modelling was performed. In the 'first approach mode' of SWISS-MODEL server, the 3D model of PchEHA was automatically built based on template structure of *H. sapiens* sEH (PDB code: 1zd3A). Because the modelling template had an additional N-terminal phosphatase domain associated with the C-terminal epoxide hydrolase domain (*11*, *39*), the resulting structure of PchEHA with a disordered N-terminal was discarded.

Therefore, the protein-sequence alignment of PchEHA and other soluble EHs whose 3D structures have been resolved, were constructed (Fig. 1), which revealed many common features, such as the catalytic triad (Asp105, Asp277 and His308 in PchEHA), two tyrosine residues (Tyr159 and Tyr241 in PchEHA), two conserved motifs H–G–X–P (X = any residue, His35–Gly36–Asn37–Pro38 in PchEHA) and G–X–Sm–X–S/T (Sm = small residue, X = any residue, Gly65–Tyr66–Gly67–Asp68–Thr69 in PchEHA), etc. However, there was the closest distance between PchEHA and *A. radiobacter* AD1 sEH (*28*) so that the 3D structure of PchEHA was successfully constructed with its X-ray structure (PDB code: 1ehyA) using the 'alignment mode' of SWISS-MODEL server. The superimposition of backbones of PchEHA with *A. radiobacter* AD1 sEH protein yielded the root mean squared deviation (RMSD) value of 0.52 Å, which indicated that the model was acceptable and reliable. Totally, the model was well in accordance with the 'canonical' α/β hydrolase-fold family. It can be divided into two domains: a core domain that is composed of the central 8 β-sheets (7 parallel strands and 1 antiparallel strand) flanked by 6 α-helixes, and a

Fig. 1 Sequence alignment of PchEHA with other soluble EHs. The sequences were retrieved from the PDB, included 1zd3A, *H. sapiens* sEH; 1cqzA, *Mus musculus* sEH; 2e3jA, *M. tuberculosis* sEH; 2cjpA, *Solanum tuberosum* sEH; 1ehyA, *A. radiobacter* AD1 sEH and PchEHA, *P. chrysosporium* sEH (GenBank: EU348855). The residues that form the putative active sites are indicated by Nu (nucleophile), A (acidic residue), H (histidine) and Y (tyrosine). NC-loop and cap-loop are shadowed and boxed, respectively. The α-helixes and β-sheets of PchEHA were underlined.

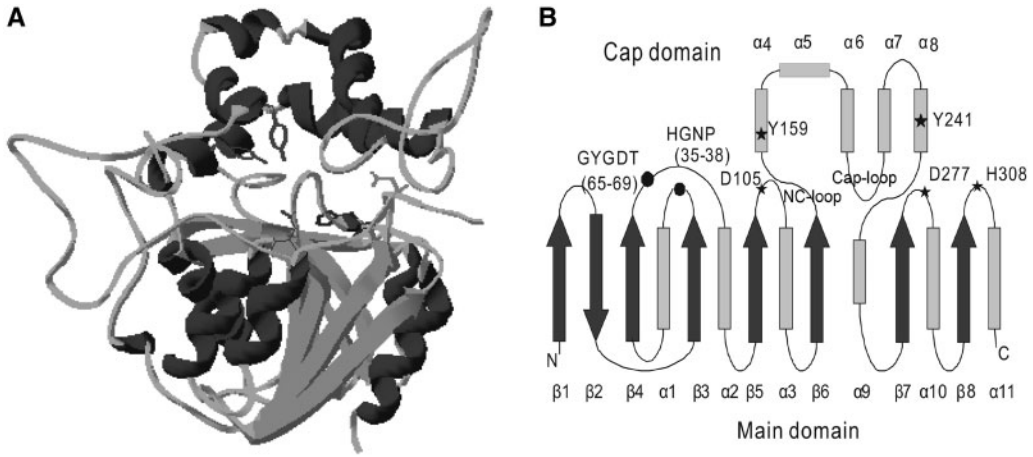

Fig. 2 Structural model and topology diagram of secondary structure of PchEHA. (A) The 3D structural model of PchEHA with the catalytic triad (D105–H308–D277) and two tyrosine residues (Y159 and Y241). (B) General topology of PchEHA. The upper part is the cap domain with 5 α-helixes (α4–α8); and the lower part is the core domain including 8 β-sheets (β1–β8) and 6 α-helixes (α1–α3 and α9–α11).

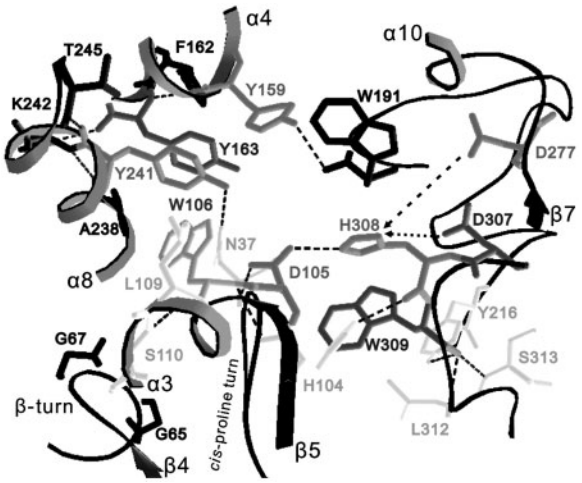

Fig. 3 The putative active site cavity of PchEHA lined with the active sites and their vicinal residues. The hydrogen-bonding interactions are shown by dotted lines.

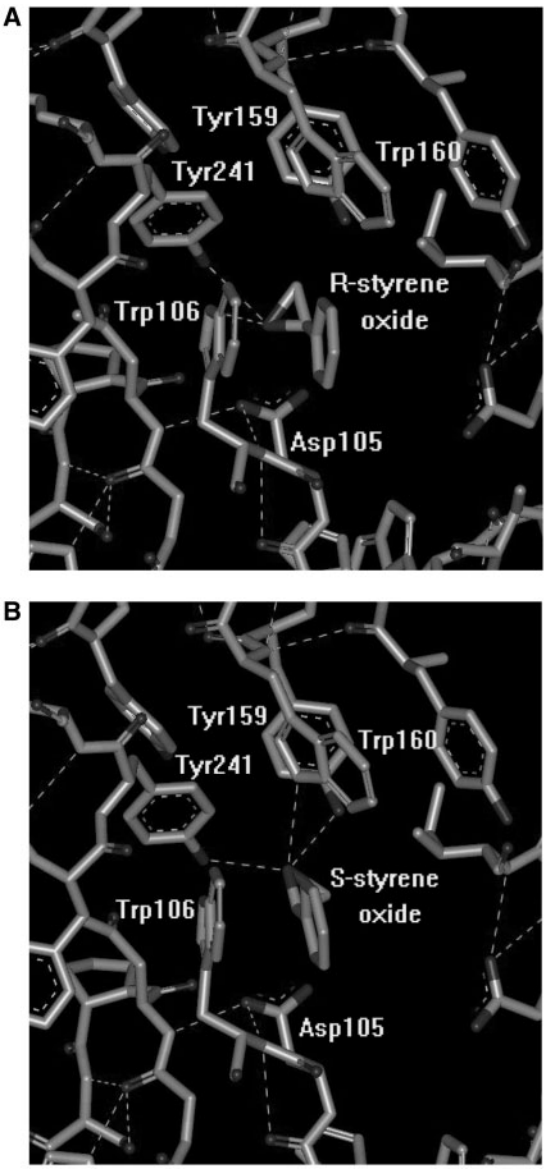

Fig. 4 Docking of styrene oxide into the active centre of PchEHA. (A) (*R*)-enantiomer; (B) (*S*)-enantiomer. Hydrogen bonds were displayed as dashed lines.

double-layered cap domain with 5 α-helixes (Fig. 2). However, the difference between the 3D model and the template is the length of NC-loop and cap-loop. The NC-loop and cap-loop of PchEHA is localized between 130–157 and 188–218, respectively. Accordingly, the PchEHA should been classified as the cluster I group that possesses the medium-sized NC-loop (16–40 residues) and long cap-loop (31–59 residues) (*16*). Finally, the putative active site cavity composed of many residues was identified around the cap domain and the core domain (Fig. 3).

Molecular docking was further carried out and tried to deeply probe the interactions between the enantiomers of SO and the amino acid residues in the PchEHA active cavity. The results showed that enantiomers of the SO were successfully docked into the active cavity (Fig. 4) with almost the same free energy, 54.08 kcal/mol and 54.99 kcal/mol for (*R*)- and (*S*)-enantiomer, respectively. However, the poses of (*S*)- and (*R*)-enantiomer of SO in the active cavity is different, leading to the distance of Asp105 to the (*R*)-enantiomer is closer than that to (*S*)-enantiomer.

Therefore, (*R*)-enantiomer of SO, preferred to be hydrolyzed by PchEHA (*28*), is easier than the (*S*)-enantiomer to interact with the attacking residue of Asp105. In addition, (*R*)-enantiomer interacts directly with Tyr159 and Trp160 via hydrogen bond (Fig. 4A), whereas (*S*)-enantiomer interacts with Tyr159 and Tyr241 via hydrogen bond in the docking model (Fig. 4B).

Generation and purification of the wt and mutant enzymes

On the model of PchEHA, a putative active site cavity composed of several residues was identified (Fig. 3). After considering the multiple sequence alignment, the following conserved residues (Asp105, Trp106, Tyr159, Tyr241, Asp277, Asp307, His308, Trp309, His35, Gly36, Asn37, Pro38, Gly65 and Gly67) were selected for investigation of their roles in the catalytic activity and enantioselectivity via site-directed mutagenesis.

All the wt and mutant enzymes were well expressed in *E. coli* BL21 (DE3) cells under the condition as described in 'Materials and Methods' section. However, for the three mutants of G36L, G65I and G67I, the recombinant proteins aggregated into the inclusion body (data not shown). Many efforts had been made to improve the soluble fraction but failed. It is possible that these changes from glycine to leucine/isoleucine at the three sites caused misfolding or conformational disorder. The recombinant proteins from the wt and other mutants were largely expressed in soluble form.

After cell disruption and centrifugal separation, the recombinant proteins from the supernatant were purified by affinity chromatography using a Ni^{2+}-chelated HisTrap FF Crude 1 ml column. The purified proteins were analysed on 12.5% SDS–PAGE gel with Coomassie Brilliant Blue staining (Fig. 5). The purity of proteins was estimated to account for >85%, except for the three mutants of G36L, G65I and G67I that showed to be impure as revealed on the SDS–PAGE gel due to poor expression in soluble form.

Hydrolytic activities of the wt and mutants

To determine the impacts of the mutants on hydrolytic activity, racemic, (*R*)- and (*S*)-SO and (*R*)- and (*S*)-GT were chosen as substrates. After terminating the reaction, the concentration of product was measured and shown in Fig. 6. The results demonstrated the wt was prone to hydrolysze (*R*)-SO and (*S*)-GT, indicating that the enantioselectivity varied towards different epoxides.

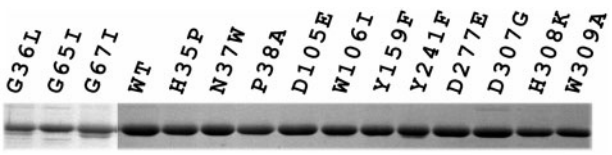

Fig. 5 SDS–PAGE analysis of the purified PchEHA wt and mutant proteins. The wt and mutant proteins were purified by affinity chromatography and loaded on the 12.5% SDS–PAGE stained with Coomassie Brilliant Blue.

In comparison with the wt, 14 mutants gave rise to different impact on the hydrolytic activity. The wt hydrolyszed 54.58%, 81.93%, 27.62% of racemic, (*R*)- and (*S*)-SO, respectively (Fig. 6A). D307G had similar activity to (*R*)-SO, but it catalysed more racemic and (*S*)-SO to its corresponding diol; N37W, D277E retained >50% of the wt hydrolytic activity; the hydrolytic percentage of H35P, W106I and W309A was about 10–25%; G36L, G65I, G67I, P38A, D105E, Y159F, Y241F and H308K had much weaker activity. It is noted that W106I preferred (*S*)-SO to (*R*)-SO, which is contrary to the wt and other mutants.

When GT was used as the substrate, almost no detectable hydrolytic activity was observed with P38A, D105E, Y159F and H308K; the wt hydrolyszed 95.92% and 25.95% of (*S*)- and (*R*)-GT; the other mutants almost did not hydrolyse (*R*)-GT (Fig. 6B). In terms of (*S*)-GT, the hydrolytic percentage of H35P, G36L, N37W, G65I, G67I, W106I, Y241F, D277E, D307G and W309A were 19.69%, 55.40%, 42.81%, 48.76%, 26.10%, 27.01%, 12.67%, 78.75%, 99.36% and 48.00%, separately. On the whole, the activity of D307G was close to the wt, but it hydrolyszed less (*R*)-GT; P38A, D105E, Y159F and H308K were nearly inactive; the other mutants retained hydrolytic activity at certain extent.

Especially, G36L, G65I and G67I recovered from the supernatant had some residual activities to all kinds of SO and (*S*)-GT, indicating that the three mutants yielded an impact on not only the protein folding but also the catalytic activity.

Hydrolytic kinetics of the wt and mutants

To further investigate the roles of these residues, the kinetic characterizations of the wt and several mutants with the racemic, (*R*)- and (*S*)-SO were calculated. Overall, the hydrolytic kinetics of the wt and these mutants was typically following the first-order reaction. For example, the hydrolytic time courses for the wt and mutants of D277E and N37W were presented in Fig. 7A. Finally, the steady-state kinetic parameters were calculated for the wt and mutants of H35P, N37W, W106I, D277E, D307G, W309A (Table I). When racemic- SO was used as the substrate, the Michaelis constant (K_m) of H35P, N37W, W106I, D277E and W309A showed a significant decline; and the specificity constant (k_{cat}/K_m) were reduced to 2.8%, 18.4%, 20.9%, 16.1% and 26.6%, respectively, in comparison with the wt. But D307G had a similar catalytic constant (k_{cat}) and a 1.14-fold catalytic efficiency (k_{cat}/K_m) compared with the wt. The K_m of H35P and N37W was ×2.74 and ×1.36 times than that of wt. While the K_m of W106I, D277E, D307G and W309A decreased slightly.

With the substrate of (*R*)-SO, all six mutants had lower k_{cat} and k_{cat}/K_m, and higher K_m-values except D277E and W309A. With (*S*)-SO as substrate, the K_m, k_{cat} and k_{cat}/K_m of D307G were greater than that of wt. W106I also had a increased k_{cat}; the other mutants showed lower k_{cat} and k_{cat}/K_m. The K_m of N37W, W106I and D277E jumped to 2.2- to 4.6-fold

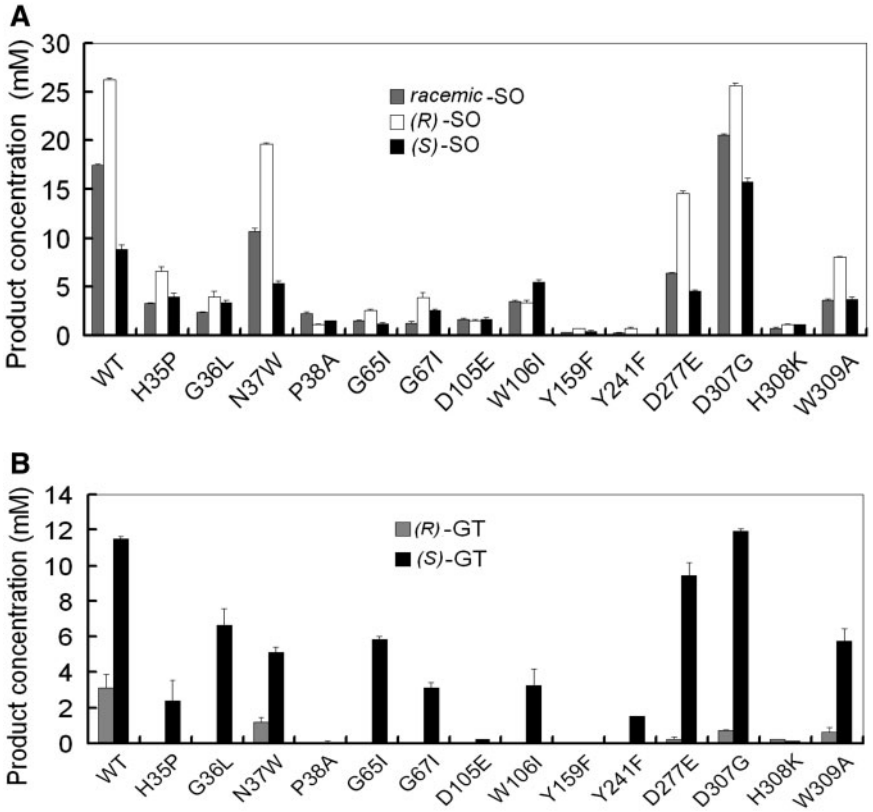

Fig. 6 Hydrolytic activity of PchEHA wt and mutants to styrene oxide and glycidyl tosylate. (A) The hydrolytic reactions were carried out in 50 µl of 10 mM phosphate buffer (pH 8.0) containing 32 mM racemic, (*R*)- or (*S*)-SO and 15 µg purified enzymes at 37°C for 30 min. (B) Hydrolysis were performed at 37°C for 1 h using 20 µg of purified enzyme and 12 mM (*R*)-, or (*S*)-GT in 50 µl of 100 mM phosphate buffer (pH 8.0).

of that of the wt. And the K_m of H35P, D307G and W309A were also higher than that of the wt.

Because of the much weaker activities of P38A, D105E, Y159F, Y241F and H308K mutants (Fig. 6A), their steady-state kinetic parameters were not determined. However, the time courses of their hydrolytic reaction to (*R*)- and (*S*)-SO was determined as described in 'Materials and Methods' section. The pattern of hydrolytic course is somehow different among these mutants. For Y241F and H308K, the hydrolytic reaction was in burst at the beginning and then quickly entered the plateau (Fig. 7B). This kinetic behaviour was obviously different from that of the other mutants, such as Y159F that showed a continuous slowly increasing (Fig. 7B). With mutants of G36L, G65I, G67I, no further kinetics assay was performed due to the limited quantities of the recombinant proteins.

Effects of mutants on enantioselectivity

The enantioselectivity of the wt and mutants were estimated by their *E*-values, which were determined by two different ways as described in 'Materials and Methods' section. For most of the mutants, the *E*-value was declined, indicated that their enantioselectivity was decreased towards SO (Table II). However, D277E and W309A increased the enantioselectivity to some extent in comparison with that of the wt. D277E showed a large increase in K_m for (*S*)-enantiomer (Table I). The resulting k_{cat}/K_m was decreased more for the slower reacting enantiomer than the preferred (*R*)-enantiomer, leading to enantioselectivity increasing. With W309A, the reduced extent of k_{cat} for the two enantiomers was similar, so the enhanced enantioselectivity was caused by the decreased K_m for (*R*)-enantiomer and the increased K_m for (*S*)-enantiomer (Table I).

It is interested that the enantioselectivity of W106I towards styrene epoxide reversed. W106I was prone to hydrolyze the (*S*)-enantiomer in contrary to the wt and other mutants (Table II), although the *E*-value was largely declined. The inverted enantioselectivity of W106I was resulted from 2- to 3-fold increase of the K_m for both enantiomers of SO, and a dramatic decrease of the k_{cat} for the (*R*)-enantiomer and a small increase of the k_{cat} for the (*S*)-enantiomer (Table I). D307G gave a k_{cat}-value for the (*S*)-enantiomer that was ~2-fold greater than that of the wt (Table I). Further, the k_{cat}/K_m of D307G for (*R*)-SO was reduced to about a half of the wt. These changes of kinetic parameters for D307G led to a significant change in the *E*-value. The small decreased enantioselectivity of N37W was mainly due to the discrepancy in K_m for (*R*)- and (*S*)-SO (Table I). About 10-fold decreased k_{cat} and 3-fold increased K_m of H35P for (*R*)-SO caused the k_{cat}/K_m decreased dramatically, so that its enantioselectivity was inconspicuous.

The *E*-values of P38A, D105E, Y159F, Y241F and H308K were simply calculated by the ratio of two initial velocities of the hydrolytic course of the separate

enantiomers (*38*). However, the *E*-value for these mutants was largely reduced to the range from 1 to 2 (Table I), perhaps due to their much low activity to both enantiomers of SO. It is suggested that these mutants lost the enantioselectivities towards SO significantly.

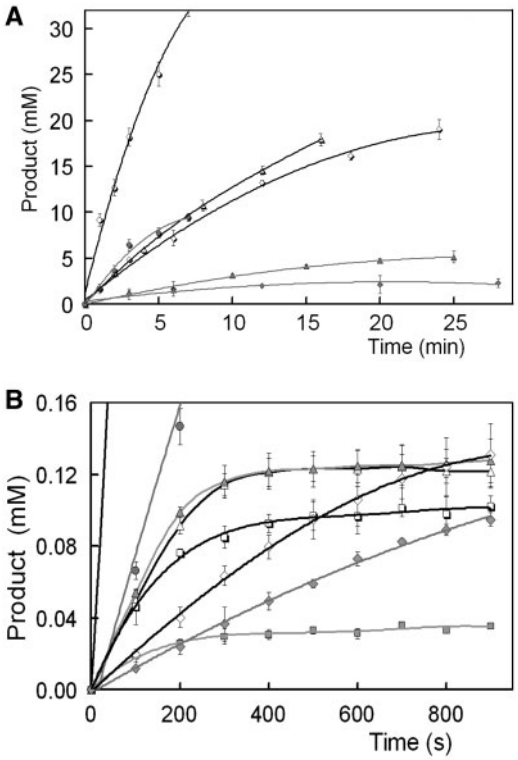

Fig. 7 Hydrolytic course of the selected mutants and wt of PchEHA. (A) A master mixture was set-up in 10 mM phosphate buffer (pH 8.0) containing 50 mM of (*R*)- or (*S*)-SO at 37°C, and then each 50 µl of the reaction mixture was withdrawn at regular intervals and used for determination of concentration of the diol product by oxidation with $NaIO_4$. The open circle with black line, wt to (*R*)-SO; grey circle with grey line, wt to (*S*)-SO; open triangle with black line, D277E to (*R*)-SO; grey triangle with grey line, D277E to (*S*)-SO; open diamond with black line, N37W to (*R*)-SO; grey diamond with grey line, N37W to (*S*)-SO. (B) The hydrolytic reaction was performed to continuously monitor the product of diol oxidation with $NaIO_4$ on line in 10 mM of phosphate buffer containing 2 mM of substrate and 50 µg of purified enzyme. The open circle with black line, wt to (*R*)-SO; grey circle with grey line, wt to (*S*)-SO; open triangle with black line, Y241F to (*R*)-SO; grey triangle with grey line, Y241F to (*S*)-SO; open diamond with black line, Y159F to (*R*)-SO; grey diamond with grey line, Y159F to (*S*)-SO; open square with black line, H308K to (*R*)-SO; grey square with grey line, H308K to (*S*)-SO.

Discussion

As well known for the classical epoxide hydrolase, hydrolytic reaction is mediated by the catalytic triad Asp–His–Asp/Glu and two Tyr residues. It occurs through a covalent enzyme–substrate intermediate stabilized by hydrogen bonds with several main-chain amide groups from the so-called oxyanion hole. In addition, the reaction may be associated with the conserved HGNP motif and several residues in the vicinity of the active sites. Our homology model of PchEHA shows an intact and empty active site cavity (Fig. 3), which is lined with many residues at least including Asp105, Trp106, Tyr159, Tyr241, Asp277, Asp307, His308, Trp309 and the HGXP motif. So these conserved residues were chosen and used to probe their roles in catalytic reaction via site-directed mutagenesis in PchEHA.

The active site cavity

According to structural model of the PchEHA, the active site cavity is located in a predominantly

Table II. Enantioselectivity of wt and 11 mutants of PchEHA towards styrene oxide.

Enzyme	*E*-value
WT	10.5(R)[a]
H35P	1.50(R)[a]
N37W	7.56(R)[a]
P38A	1.55(R)[b]
D105E	1.88(R)[b]
W106I	2.62(S)[a]
Y159F	1.85(R)[b]
Y241F	1.17(S)[b]
D277E	12.3(R)[a]
D307G	4.02(R)[a]
H308K	1.75(R)[b]
W309A	13.4(R)[a]

[a]For PchEHA wt and mutants of H35P, N37W, W106I, D277E, D307G and W309A, the *E*-value is calculated from the ratio of k_{cat}/K_m values of two separate enantiomers. The preferentially hydrolyzed enantiomer is indicated in parentheses.
[b]For mutants of P38A, D105E, Y159F, Y241F and H308K, the *E*-value is the ratio of the hydrolysis curve slope of two enantiomers. The enantiomer that is preferentially hydrolyzed is indicated in parentheses.

Table I. Steady-state kinetic parameters PchEHA wt and several mutants for racemic, (*R*)- and (*S*)-styrene oxide[a].

	Racemic			(*R*)-styrene oxide			(*S*)-styrene oxide		
	k_{cat}	K_m	k_{cat}/K_m	k_{cat}	K_m	k_{cat}/K_m	k_{cat}	K_m	k_{cat}/K_m
WT	7.94	25.1	0.316	12.97	13.5	0.961	1.38	15.1	0.091
H35P	0.65	68.8	0.009	1.35	41.3	0.033	0.41	18.6	0.022
N37W	1.96	34.1	0.058	3.14	23.1	0.136	0.82	46.8	0.018
W106I	1.33	20.1	0.066	0.82	39.5	0.021	1.81	33.0	0.055
D277E	1.08	21.2	0.051	1.62	11.1	0.147	0.82	68.4	0.012
D307G	7.04	19.5	0.361	10.95	19.3	0.567	2.56	18.2	0.141
W309A	1.35	16.1	0.084	1.59	11.9	0.134	0.17	16.3	0.010

[a]The units of kinetic parameters: k_{cat}, s^{-1}; K_m, mM; k_{cat}/K_m, $mM^{-1}\,s^{-1}$; these parameters were calculated using the mean values from three independent experiments.

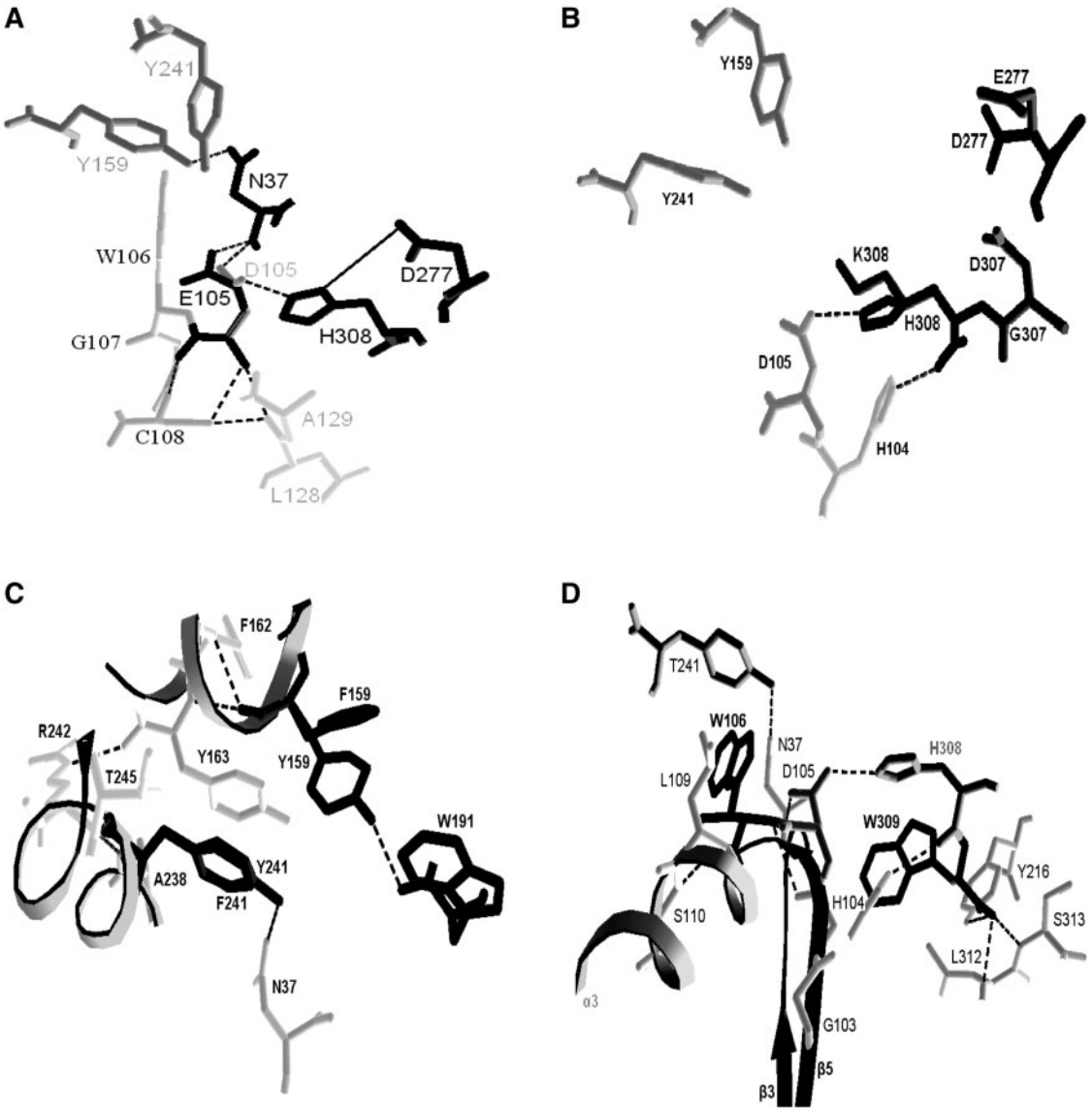

Fig. 8 Local view of the selected residues and their mutated partners in PchEHA structural model. The hydrogen-bonding interactions are shown by dotted lines. (A) D105 and the mutant E105 with the coordinating or interacting residues. (B) D277, D307 and H308 and their mutated partners. (C) Y159 and Y241 with their interacting residues. (D) W106 and W309 and their interacting residues.

hydrophobic environment, between the core and the cap domain. The residues that consist of the putative catalytic triad, Asp105–His308–Asp277, are lined up in a row on the side of the active site cleft, with Asp105 taking the innermost position in the cleft, and Asp277 found nearest the surface of the protein (Fig. 2A). In addition, two tyrosine residues directly interact with the substrate of SO in the docking model (Fig. 4).

Mutation of Asp105 resulted in a dramatic loss of enzyme activities for SO and GT (Fig. 6), indicating that Asp105 is involved in catalysis which is consistence with our structural model (Fig. 8A) and the previous studies. For examples, replacement of the corresponding Asp with a non-functional amino acid also leads to a complete loss of enzymatic activity (*5*, *6*, *10*, *40*, *41*). These results confirm that the nucleophile Asp105 plays a primary role in initiating enzymatic activity by nucleophilic attack. Further, the distance between Asp105 and epoxide ring of the substrate may determine the regiospecificity because the distance of attacking Asp105 is slightly closer to the preferred (*R*)-enantiomer than that to (*S*)-enantiomer as shown in this docking model (Fig. 4), which has been suggested to explain some mutants with increased enantioselectivity (*26*).

Mutation of His308 causes the loss of imidazole group, whose Nε2 atom has been suggested to activate the water molecule in the hydrolysis of ester intermediate (Fig. 8B). As expected, the replacement of His308 with Lys led to much weak activity (Fig. 6). Further, the hydrolytic progress of SO was likely a single turnover reaction with a burst for a short time and then stopped (Fig. 7B). This kinetic behaviour may be ascribed to accumulation of a covalent ester intermediate. Since the enzymatic reaction has been demonstrated to be covalently trapped with the mutant H275R of *A. radiobacter* sEH, the covalent ester

intermediate accumulated and no diol was produced (*6*). Similarly, several mutants of the corresponding His in other EHs displayed <1% of the wt enzyme activities (*5*, *6*, *10*, *40–42*). All the evidences suggested that the His residue in catalytic triad is the general base involved in water activation and its imidazole group is related to alkylation and hydrolysis steps.

The proposed acidic member of catalytic triad, Asp277 is located in a turn between strand β7 and helix α10 (Fig. 2B). Its function is possible to assist His308 in the hydrosis step. However, Asp277 in the structural model of PchEHA is beyond the interacting distance of His308. Well, a hydrogen bond was formed between the corresponding residues of Asp495 and His523 in *M. musculus* sEH (*17*). Although the k_{cat} and k_{cat}/K_m of D277E decreased drastically, it still had some residual activities for SO and GT. This is consistent with D348E of *A. niger* sEH and D285E of soybean sEH (*40*, *41*). D348E of *A. niger* sEH caused a reduce of the V_{max} by half and a significant drop in K_m by a factor of 3, indicating that D348E switched the rate-limiting step in the enzymatic reaction (*40*). In some microsomal EHs containing a glutamate as the acidic residue, there is the reverse relationship between wt and their Glu–Asp mutants (*13*, *43*). These indicate the importance of the Asp residue in catalysis but not essential.

In the structure model, another Asp307 is positioned close to His308 and in the same direction with Asp277 (Fig. 8B). The mutagenesis studies have revealed that D307G had similar activity with the wt, but its *E*-value fell to 4.02 from 10.5. On the contrary, the D277E mutant had lower activity and higher enantioselectivity. Therefore, Asp307 may act as a backup of Asp277 based on the structure and the complementarity of their kinetic parameters. A similar shift of functional residues has been observed for EHs from *A. radiobacter*, soybean and rat (*41*, *43*, *44*). Although the backup of charge relay residue does not play a decisive role in catalysis, it affects the enzymatic reaction.

In the light of multiple sequence alignment and structural model of PchEHA, two conserved tyrosines, Tyr159 and Tyr241, are identified in the first and the fifth α-helix of the cap domain (Fig. 2). They are positioned towards the nucleophilic Asp105 and protruded into the active cavity (Fig. 8C). Furthermore, the molecular docking has been demonstrated that those two tyrosine residues directly interact with the substrate of SO (Fig. 4). Therefore, they may facilitate the opening of the epoxide ring by hydrogen bonding and protonating the epoxide oxygen. To verify this hypothesis, mutants of Y159F and Y241F were constructed. In the absence of substrates, the phenolic hydroxyl group of Tyr159 is stabilized by the main chain of Trp191 and towards the interface of the core and the cap domain (Fig. 8C). But the phenyl group of Phe159 turned towards the cap domain. Although the orientation of the Phe241 did not change, it cannot offer a hydroxyl group (Fig. 8C). As a result, Y159F and Y241F failed to engage in formation of hydrogen bonding and proton donation with substrates. As expected, both of the mutants (Y159F and Y241F) were almost inactive. However, their roles in catalytic mechanism may be different as demonstrated by the hydrolytic course (Fig. 7B). Since Y241 interacts with the oxygen hole (Asn37), Y241F may weaken the stability of intermediate, consequently leading to the hydrolysis of intermediate to decline quickly. The mutations of the corresponding residues in sEH from potato, soybean and murine also cause a dramatic loss of activity by decreasing the rate of binding substrate and formation of an intermediate (*8*, *10*, *41*). However, our results is somehow different from the two mutants of Y152F and Y215F of *A. radiobacter* AD1 sEH (*45*, *46*), which retained moderate activity. Conclusively, the two tyrosines are essential to retain reasonable catalytic activity.

Site-directed mutagenesis was performed individually on the other two residues, Trp106 and Trp309, because of their vicinity to the catalytic triad (Fig. 8D). In EHs, the residue next to the active site nucleophile is not strictly conserved, but it is often a tryptophan, such as the Trp106 in PchEHA (Fig. 1). The corresponding residue was Phe108 in sEH from *A. radiobacter*, which has been investigated deeply by saturation mutagenesis (*27*). Mutants at this position have a huge impact on the activity and enantioselectivity. To phenyl glycidyl ether and *p*-nitrostyrene oxide, the enantioselectivity of F108C was contrary to that of the wt. The effect of W106I on the catalysis is expected in the PchEHA (Table I). Especially, the k_{cat} for (*S*)-SO was higher than k_{cat} for racemic and (*R*)-enantiomer, leading to an opposite enantioselectivity (Table II). In the docking model, Trp106 directly interacts with the preferred (*R*)-enantiomer of SO, but not with (*S*)-enantiomer (Fig. 4A). So, mutant W160I may weaken the substrate binding much seriously to the preferred enantiomer of (*R*)-SO, as shown its K_m (=39.5 mM) increased about three times over the wt (Table I). The resulting k_{cat} of W160I for (*R*)-SO is greatly reduced for about 15-fold in comparison with the wt, while the k_{cat} of W160I for (*S*)-SO is slightly decreased (Table I). Taken together, the converted enantioselctivity of W106I may be due to much deteriorative effect on the preferred enantiomer of (*R*)-SO. In addition, the amide proton of Leu106 still contributes to the oxyanion hole as Trp106 does (Fig. 8D), Trp106 in PchEHA is inferred to influence substrate binding, especially for the preferred (*R*)-enantiomer.

For the similar reason, Ala309 may not maintain the integrity of the active site cavity (Fig. 8D) and therefore lead to the activity of W309A decreased seriously to both enantiomers. Consequently, the neighbouring residues of active site may change the shape of substrate channel and influence the activity and enantioselectivity of PchEHA.

H35P, G36L, N37W and P38A mutants

The HGXP motif between strand β3 and helix α1 is one of distinguishing characteristics of EHs and haloalkane dehalogenases (*20*). However, few studies were focused on this motif. In the PchEHA structural model, this motif forms a sharp *cis*-proline turn (Asn37-Pro38), and is protruded into the active site

cavity. Residue X is usually an aromatic amino acid in most EHs (Fig. 1). In the case of PchEHA, it is an exception that the X residue is an asparagine. Along the *cis*-proline reverse turn, the main chain amide of Asn37 aims at the active sites, and the side chain amido forms a hydrogen bond with the phenolic hydroxyl group of Tyr241 (Fig. 8C). The indolyl of mutant N37W is close to Tyr241 but lose the hydrogen bond in the 3D structure. With racemic, (*R*)- and (*S*)-SO as substrates, the K_m of N37W was a bit higher than the wt, but the values of k_{cat} and k_{cat}/K_m decreased markedly. In rat mEH, the corresponding residue Trp150 has been shown to contribute to reduce the change in intrinsic fluorescence of the protein during alkylation (*43*). Taken together, Asn37 in PchEHA is suggested to coordinate the active site cavity.

In point of structural model, mutations of Gly36 and Pro38 may disrupt the *cis*-turn structure. The replacement of Gly36 to Leu resulted in aggregation of the recombination protein in *E. coli*, perhaps due to no room for the larger side chain alkyl. The activity of P38A was seriously reduced (Fig. 6). H35P also presented much weaker activity, with the k_{cat}/K_m value only about 3% of the wt for racemic, (*R*)-SO (Table II). The corresponding mutant of H148N in rat mEH has been shown to affect the conformation of active sites and reduce the activity, while H148L mutant was poorly expressed (*42*). So these mutations may cause the disintegration of *cis*-proline turn and further lead to structural perturbation of the active site cavity.

G65I and G67I mutants

The N-terminally located G–X–Sm–X–S/T motif is another indicator to annotate the putative EH sequences. However, its function is unknown (*20*). According to multiple sequence alignment, the first X is an aromatic residue and the Sm is a glycine (Fig. 1). In the PchEHA model, the GYGDT motif is part of a large loop-linking strand β4 and helix α2. The loop has three β-turns ascribed to Gly65, Gly67 and Pro75, separately. The overall turn potentials for Gly and Pro are highest, indicating their preference to occurring in β-turns (*47*). The lack of side chain makes Gly a suitable amino acid to well adjust the steric hindrances of other residues in the β-turns. The main roles of β-turns have been suggested to change the direction of protein chain, facilitate the recognition and interaction between protein donors and receptors, and ensure the correct folding and conformational stability of proteins (*47*, *48*). Because G65I and G67I mutants were expressed in the form of inclusion body, the two β-turns are supposed to be necessary for protein folding correctly in PchEHA.

Supplementary Data

Supplementary Data are available at *JB* Online.

Funding
The HiTech Research and Development Program of China (2006AA02Z221 to H.F.).

Conflict of interest
None declared.

References

1. Arand, M., Cronin, A., Adamska, M., and Oesch, F. (2005) Epoxide hydrolases: structure, function, mechanism and assay. *Methods Enzymol.* **400**, 569–588
2. Morisseau, C. and Hammock, B.D. (2005) Epoxide hydrolases: mechanisms, inhibitor designs, and biological roles. *Annu. Rev. Pharmacol. Toxicol.* **45**, 311–333
3. Decker, M., Arand, M., and Cronin, A. (2009) Mammalian epoxide hydrolases in xenobiotic metabolism and signalling. *Arch. Toxicol.* **83**, 297–318
4. Archelas, A. and Furstoss, R. (2001) Synthetic applications of epoxide hydrolases. *Curr. Opin. Chem. Biol.* **5**, 112–119
5. Pinot, F., Grant, D.F., Beetham, J.K., Parker, A.G., Borhan, B., Landt, S., Jones, A.D., and Hammock, B.D. (1995) Molecular and biochemical evidence for the involvement of the Asp-333-His-523 pair in the catalytic mechanism of soluble epoxide hydrolase. *J. Biol. Chem.* **270**, 7968–7974
6. Rink, R., Fennema, M., Smids, M., Dehmel, U., and Janssen, D.B. (1997) Primary structure and catalytic mechanism of the epoxide hydrolase from *Agrobacterium radiobacter* AD1. *J. Biol. Chem.* **272**, 14650–14657
7. Nardini, M., Ridder, I.S., Rozeboom, H.J., Kalk, K.H., Rink, R., Janssen, D.B., and Dijkstra, B.W. (1999) The X-ray structure of epoxide hydrolase from *Agrobacterium radiobacter* AD1. An enzyme to detoxify harmful epoxides. *J. Biol. Chem.* **274**, 14579–14586
8. Yamada, T., Morisseau, C., Maxwell, J.E., Argiriadi, M.A., Christianson, D.W., and Hammock, B.D. (2000) Biochemical evidence for the involvement of tyrosine in epoxide activation during the catalytic cycle of epoxide hydrolase. *J. Biol. Chem.* **275**, 23082–23088
9. van Loo, B., Lutje Spelberg, J.H., Kingma, J., Sonke, T., Wubbolts, M.G., and Janssen, D.B. (2004) Directed evolution of epoxide hydrolase from *A. radiobacter* toward higher enantioselectivity by error-prone PCR and DNA shuffling. *Chem. Biol.* **11**, 981–990
10. Elfstrom, L.T. and Widersten, M. (2005) Catalysis of potato epoxide hydrolase, StEH1. *Biochem. J.* **390**, 633–640
11. Gomez, G.A., Morisseau, C., Hammock, B.D., and Christianson, D.W. (2006) Human soluble epoxide hydrolase: structural basis of inhibition by 4-(3-cyclohexylureido)-carboxylic acids. *Protein Sci.* **15**, 58–64
12. Mowbray, S.L., Elfstrom, L.T., Ahlgren, K.M., Andersson, C.E., and Widersten, M. (2006) X-ray structure of potato epoxide hydrolase sheds light on substrate specificity in plant enzymes. *Protein Sci.* **15**, 1628–1637
13. Liu, Y., Wu, S., Wang, J., Yang, L., and Sun, W. (2007) Cloning, expression, purification and characterization of a novel epoxide hydrolase from *Aspergillus niger* SQ-6. *Protein Expr. Purif.* **53**, 239–246
14. Luo, Q., Yao, Y., Han, W.W., Zhou, Y.H., and Li, Z.S. (2009) Homology modeling of a novel epoxide hydrolase (EH) from *Aspergillus niger* SQ-6: structure-activity relationship in expoxides inhibiting EH activity. *J. Mol. Model.* **15**, 1125–1132
15. Ollis, D.L., Cheah, E., Cygler, M., Dijkstra, B., Frolow, F., Franken, S.M., Harel, M., Remington, S.J., Silman, I., Schrag, J., Sussman, J.L., Verschueren, K.H.G., and

Goldman, A. (1992) The α/β-hydrolase fold. *Protein Eng.* **5**, 197–211
16. Barth, S., Fischer, M., Schmid, R. D., and Pleiss, J. (2004) Sequence and structure of epoxide hydrolases: a systematic analysis. *Proteins* **55**, 846–855
17. Argiriadi, M.A., Morisseau, C., Hammock, B.D., and Christianson, D.W. (1999) Detoxification of environmental mutagens and carcinogens: structure, mechanism, and evolution of liver epoxide hydrolase. *Proc. Natl Acad. Sci. USA* **96**, 10637–10642
18. Zou, J., Hallberg, B.M., Bergfors, T., Oesch, F., Arand, M., Mowbray, S.L., and Jones, T.A. (2000) Structure of *Aspergillus niger* epoxide hydrolase at 1.8 Å resolution: implications for the structure and function of the mammalian microsomal class of epoxide hydrolases. *Structure* **8**, 111–122
19. Biswal, B.K., Morisseau, C., Garen, G., Cherney, M.M., Garen, C., Niu, C., Hammock, B.D., and James, M.N.G. (2008) The molecular structure of epoxide hydrolase B from *Mycobacterium tuberculosis* and its complex with a urea-based inhibitor. *J. Mol. Biol.* **381**, 897–912
20. van Loo, B., Kingma, J., Arand, M., Wubbolts, M.G., and Janssen, D.B. (2006) Diversity and biocatalytic potential of epoxide hydrolases identified by genome analysis. *Appl. Environ. Microbiol.* **72**, 2905–2917
21. Reetz, M.T., Torre, C., Eipper, A., Lohmer, R., Hermes, M., Brunner, B., Maichele, A., Bocola, M., Arand, M., Cronin, A., Genzel, Y., Archelas, A., and Furstoss, R. (2004) Enhancing the enantioselectivity of an epoxide hydrolase by directed evolution. *Org. Lett.* **6**, 177–180
22. Rui, L., Cao, L., Chen, W., Reardon, K.F., and Wood, T.K. (2004) Active site engineering of the epoxide hydrolase from *Agrobacterium radiobacter* AD1 to enhance aerobic mineralization of cis-1,2-dichloroethylene in cells expressing an evolved toluene *ortho*-monooxygenase. *J. Biol. Chem.* **279**, 46810–46817
23. Rui, L., Cao, L., Chen, W., Reardon, K.F., and Wood, T.K. (2005) Protein engineering of epoxide hydrolase from *Agrobacterium radiobacter* AD1 for enhanced activity and enantioselective production of (R)-1-phenylethane-1,2-diol. *Appl. Environ. Microbiol.* **71**, 3995–4003
24. Kotik, M., Stepanek, V., Kyslik, P., and Maresova, H. (2007) Cloning of an epoxide hydrolase-encoding gene from *Aspergillus niger* M200, overexpression in *E. coli*, and modification of activity and enantioselectivity of the enzyme by protein engineering. *J. Biotechnol.* **132**, 8–15
25. Choi, S.H., Kim, H.S., and Lee, E.Y. (2009) Comparative homology modeling-inspired protein engineering for improvement of catalytic activity of *Mugil cephalus* epoxide hydrolase. *Biotechnol. Lett.* **31**, 1617–1624
26. Reetz, M.T., Bocola, M., Wang, L.-W., Sanchis, J., Cronin, A., Arand, M., Zou, J., Archelas, A., Bottalla, A.-L., Naworyta, A., and Mowbray, S.L. (2009) Directed evolution of an enantioselective epoxide hydrolase: Uncovering the source of enantioselectivity at each evolutionary stage. *J. Am. Chem. Soc.* **131**, 7334–7343
27. van Loo, B., Kingma, J., Heyman, G., Wittenaar, A., Lutje Spelberg, J.H., Sonke, T., and Janssen, D.B. (2009) Improved enantioselective conversion of styrene epoxides and meso-epoxides through epoxide hydrolases with a mutated nucleophile-flanking residue. *Enzyme Microb. Technol.* **44**, 145–153
28. Li, N., Zhang, Y., and Feng, H. (2009) Biochemical characterization and transcriptional analysis of the epoxide hydrolase from white-rot fungus *Phanerochaete chrysosporium*. *Acta Biochim. Bioph. Sin.* **41**, 638–647
29. Peitsch, M.C. (1995) Protein modelling by E-mail: from amino acid sequence to protein structure: a free one-hour service. *Nat. Biotechnol.* **13**, 658–660
30. Guex, N. and Peitsch, M.C. (1997) SWISS-MODEL and the Swiss-PdbViewer: an environment for comparative protein modeling. *Electrophoresis* **18**, 2714–2723
31. Schwede, T., Kopp, J., Guex, N., and Peitsch, M.C. (2003) SWISS-MODEL: an automated protein homology-modeling server. *Nucleic Acids Res.* **31**, 3381–3385
32. Yang, J-M. and Chen, C-C. (2004) GEMDOCK: A Gerneric evolutionary method for molecular docking. *Proteins: Stru. Func. Bioinform.* **55**, 288–304
33. Yang, J-M. and Shen, T-W. (2005) A pharmacophore-based evolutionary approach for screen selective estrogen receptor modulators. *Protein: Stru. Func. Bioinform.* **59**, 205–220
34. Zocher, F., Enzelberger, M.M., Bornscheuer, U.T., Hauer, B., and Schmid, R.D. (1999) A colorimetric assay suitable for screening epoxide hydrolase activity. *Anal. Chim. Acta* **391**, 345–351
35. Tang, Y.F., Xu, J.H., and Ye, Q. (2002) A spectrophotometric assay for determination of epoxide concentration and epoxide hydrolase activity. *J. Anal. Sci.* **18**, 142–144
36. Mateo, C., Archelas, A., and Furstoss, R. (2003) A spectrophotometric assay for measuring and detecting an epoxide hydrolase activity. *Anal. Biochem.* **314**, 135–141
37. Chen, C.S., Fujimoto, Y., Girdaukas, G., and Sih, C.J. (1982) Quantitative analyses of biochemical kinetic resolutions of enantiomers. *J. Am. Chem. Soc.* **104**, 7294–7299
38. Mantovani, S.M., de Oliveira, L.G., and Marsaioli, A.J. (2008) Whole cell quick *E* for epoxide hydrolase screening using fluorescent probes. *J. Mol. Catal. B: Enzym.* **52, 53**, 173–177
39. Cronin, A., Mowbray, S., Dürk, H., Homburg, S., Fleming, I., Fisslthaler, B., Oesch, F., and Arand, M. (2003) The N-terminal domain of mammalian soluble epoxide hydrolase is a phosphatase. *Proc. Natl Acad. Sci. USA* **100**, 1552–1557
40. Arand, M., Hemmer, H., Dürk, H., Baratti, J., Archelas, A., Furstoss, R., and Oesch, F. (1999) Cloning and molecular characterization of a soluble epoxide hydrolase from *Aspergillus niger* that is related to mammalian microsomal epoxide hydrolase. *Biochem. J.* **344**, 273–280
41. Blée, E., Summerer, S., Flenet, M., Rogniaux, H., Van Dorsselaer, A., and Schuber, F. (2005) Soybean epoxide hydrolase: identification of the catalytic residues and probing of the reaction mechanism with secondary kinetic isotope effects. *J. Biol. Chem.* **280**, 6479–6487
42. Bell, P.A. and Kasper, C.B. (1993) Expression of rat microsomal epoxide hydrolase in *Escherichia coli*. Identification of a histidyl residue essential for catalysis. *J. Biol. Chem.* **268**, 14011–14017
43. Tzeng, H.F., Laughlin, L.T., and Armstrong, R.N. (1998) Semifunctional site-specific mutants affecting the hydrolytic half-reaction of microsomal epoxide hydrolase. *Biochemistry* **37**, 2905–2911
44. Nardini, M., Rink, R., Janssen, D.B., and Dijkstra, B.W. (2001) Structure and mechanism of the epoxide hydrolase from *Agrobacterium radiobacter* AD1. *J. Mol. Catal. B: Enzym.* **11**, 1035–1042
45. Rink, R., Lutje Spelberg, J.H., Pieters, R.J., Kingma, J., Nardini, M., Kellogg, R.M., Dijkstra, B.W., and Janssen, D.B. (1999) Mutation of tyrosine residues involved in the alkylation half reaction of epoxide hydrolase from *Agrobacterium radiobacter* AD1 results in

improved enantioselectivity. *J. Am. Chem. Soc.* **121**, 7417–7418
46. Rink, R., Kingma, J., Lutje Spelberg, J.H., and Janssen, D.B. (2000) Tyrosine residues serve as proton donor in the catalytic mechanism of epoxide hydrolase from *Agrobacterium radiobacter*. *Biochemistry* **39**, 5600–5613
47. Hutchinson, E.G. and Thornton, J.M. (1994) A revised set of potentials for beta-turn formation in proteins. *Protein Sci.* **3**, 2207–2216
48. Rose, G.D., Gierasch, L.M., and Smith, J.A. (1985) Turns in peptides and proteins. *Adv. Protein Chem.* **37**, 100–109